Physics and chemistry of interstellar ice

Guss, K.M.R.

Chapter II

THERMAL COLLAPSE OF POROUS AMORPHOUS SOLID WATER

Thermal collapse of porous interstellar ice
J.-B. Bossa, K. Isokoski, M. S. de Valois, and H. Linnartz
Astronomy & Astrophysics, 545, A82 (2012)

Abstract

Amorphous solid water (ASW) is the major constituent of interstellar ice. Freeze-out of water onto cold grain surfaces in the interstellar medium is expected to result in porous ASW with large internal surface area. Energetic processing has been shown to decrease the porosity in laboratory ices and may explain why observations towards icy sources do not show dangling OH groups that are taken as a signature of porosity. A decrease in porosity may affect the chemical activity of the ice: collapse of porous interstellar ASW can accelerate diffusion-limited surface-reactions at low temperatures, while at elevated temperatures the surface area available for catalysis will dramatically decrease. The collapse of porous ASW therefore likely will influence the overall efficiency of solid-state processes taking place in interstellar ices. In this work we study the thermal collapse of porous ASW by direct monitoring of the ice film thickness using laser optical interference. The ASW film thickness is measured continuously during ice growth and subsequent thermal processing from 15 to 190 K. The changes in ice morphology during thermal collapse are confirmed by comparison with different ice morphologies and by FTIR spectroscopy of dangling OH groups. Thermal annealing of vapor deposited porous ASW results in a gradual and irreversible thinning of the ice layer. We derive a thinning of 12 % between 15 and 120 K, which we interpret as a collapse of the porous structure, as the thinning is accompanied by a decrease in the dangling OH groups. We demonstrate that laser optical interference, commonly used to monitor the growth of laboratory ices, is a simple and powerful tool to monitor the change in morphology of porous structures. Our experiments show that thermal collapse of porous ASW is a gradual and irreversible process which may influence the interstellar grain-surface chemistry already at very low temperatures.

2.1 Introduction

Amorphous solid water (ASW) is the main component of interstellar and cometary ices (Hagen 1981, Tielens & Allamandola 1987). It provides an environment for other species, sequentially accreted or formed via solid state astrochemical processes (Öberg et al. 2011b). Water has been experimentally shown to form from atomic hydrogen and oxygen via low-temperature grain-surface reactions (Ioppolo et al. 2008, Dulieu et al. 2010, Ioppolo et al. 2010, Cuppen et al. 2010, Romanzin et al. 2011) with a compact (non-porous) structure (Oba et al. 2009). Remote identification of morphology and, more precisely the porosity relies on relatively weak absorption features around 2.7 μm due to the dangling OH bonds of water on the surface of pores. Up to date, there is no observational evidence for the existence of dangling OH bonds in interstellar ices (Keane et al. 2001, Gibb et al. 2004) leading to a conclusion that porous ASW is rare in space. Given the diversity of the environments of interstellar ices (Kouchi & Yamamoto 1995, Gálvez et al. 2010), and the limited sample of available ice observations, the absence porosity is however not conclusive. In shock regions and outflows, the sputtering of frozen water molecules from grain mantles redistributes ice on the remaining cold surfaces that may lead to the formation

of a vapor-deposited ASW coating on grains. The main characteristic of vapor-deposited water ice is its porosity (Baragiola 2003). Porous ice is expected to be chemically more reactive as it provides large effective surface areas for catalysis, for further freeze-out of atoms and molecules, and for gas retention. Adsorption areas can be hundreds of m^2/g. As a consequence, a large amount of molecules can be stored inside pores at low temperatures influencing the efficiency of solid state astrochemical processes. In a later stage these species and eventual reaction products are thermally released (Collings et al. 2003).

In the laboratory, the morphology of ASW depends on the experimental conditions such as temperature, deposition rate and deposition direction of water molecules onto the substrate (Stevenson et al. 1999, Kimmel et al. 2001b, Dohnálek et al. 2003). Background deposition of water vapor onto a cold surface results in highly porous ASW (Stevenson et al. 1999, Kimmel et al. 2001b). After deposition, the ice morphology may change depending on external influences. A disappearance of pores has been observed in ion and UV photon irradiation experiments (Palumbo 2006, Palumbo et al. 2010, Raut et al. 2008). Furthermore, thermal annealing triggers a phase transition between 38 to 68 K (Jenniskens & Blake 1994), and makes ASW more compact by closing pores thereby trapping other co-deposited gases (Mayer & Pletzer 1986, Bar-Nun & Owen 1998, Collings et al. 2003). The mechanisms responsible for these morphological changes are not fully understood, particularly at low temperature, where diffusion of molecules is limited (Garrod et al. 2008). In previous studies a collapse of pores has also been concluded following X-ray and electron diffraction studies (Hallbrucker et al. 1989, Jenniskens et al. 1995), temperature programmed desorption (Collings et al. 2003), infrared spectroscopy (Hagen et al. 1983, Rowland & Devlin 1991, Rowland et al. 1991), internal friction (Hessinger et al. 1996) and gas adsorption experiments (Bar-Nun & Owen 1998, Kimmel et al. 2001b, Horimoto et al. 2002).

This chapter presents a new and generally applicable method yielding experimental results that directly demonstrate the thickness decrease of porous ASW upon thermal annealing. Sect. 2.2 describes details on experiment and data analysis. Sect. 2.3 presents the results obtained during deposition and thermal processing of different water ice morphologies. The discussion is given in Sect. 2.4, and includes a quantitative analysis of the experimental results followed by astrophysical implications. A summary and concluding remarks are given in the final section.

2.2 Experimental methods

Experiments are performed in a high-vacuum chamber with a base pressure of 2×10^{-7} Torr at room temperature. The experimental set-up (Fig. 2.1) has been described in detail by Gerakines et al. (1995) and has been further adapted to the configuration described here. Different water ices are grown either on a CsI window or on a silicon (Si) substrate at 15 and 140 K. The substrate is mounted on a closed-cycle helium cryostat that, in conjunction with resistive heating, allows an accurate temperature control from 15 to 300 K

with a precision of 0.1 K. We use milli-Q grade water that is further purified by three freeze-pump-thaw cycles prior to deposition. Depending on the experimental conditions, water ices with different morphology is produced: (i) porous amorphous, (ii) semi-porous amorphous, and (iii) crystalline solid water. Semi-porous ASW is obtained by deposition at 15 K by using a gas inlet (2 mm diameter) directed toward the substrate at normal angle of incidence (Kimmel et al. 2001b). Porous ASW and crystalline solid water are grown by background deposition at 15 and 140 K, respectively. In background deposition the gas inlet is directed away from the substrate, which allows the water molecules to impinge the surface with random trajectories (Stevenson et al. 1999, Dohnálek et al. 2003).

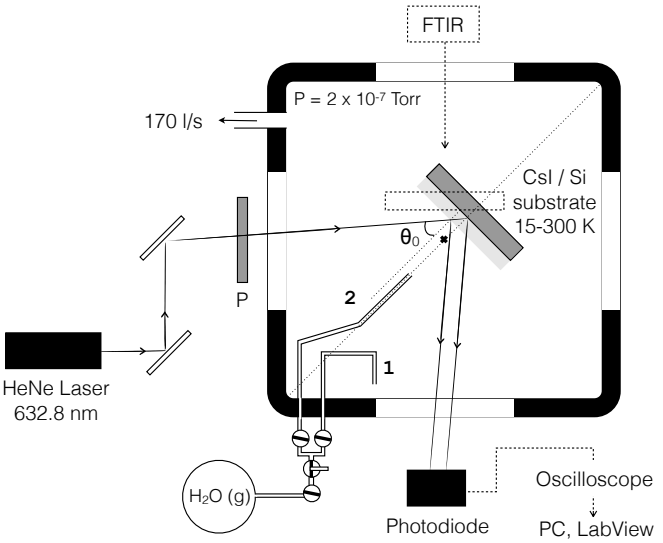

Figure 2.1 – Experimental setup used to measure thin-film interference in interstellar ice analogs. P = linear polarizer.

The ice thickness is monitored during both deposition and thermal annealing by optical interference using a linearly polarized helium-neon (He-Ne) laser. The laser beam is s-polarized (perpendicular to the plane of incidence), and strikes the substrate at an incident angle $\theta_0 = 35 \pm 5\,^\circ$. The reflected light is collected at a photodiode and digitized by an oscilloscope. A second photodiode is used prior to the vacuum chamber to monitor the laser fluctuations from scattered light. The signal is recorded as a function of time using LabVIEW 8.6 (National Instruments) software package. The ice thickness d can be expressed as a function of interference fringes (m):

$$d = \frac{\mathrm{m}\,\lambda}{2\,\mathrm{n}_1/\mathrm{n}_0\cos\theta_1}, \tag{2.1}$$

where λ corresponds to the wavelength of the laser (632.8 nm), n_0 and n_1 are the refractive indices of vacuum and ice, respectively. θ_1 is the angle of refraction related to the

angle of incidence through the Snell's law ($\sin\theta_0\ n_0 = \sin\theta_1\ n_1$). To exclude the influence of the gas deposited on the backside of the substrate, we use the Si substrate that is opaque to the laser wavelength. We use $n_0 = 1$ for vacuum, $n_1 = 1.19$ for porous ASW at 15 K (extrapolated from the data reported in Dohnálek et al. (2003)), and $n_1 = 1.29$ for semi-porous ASW (Westley et al. 1998). The ice thickness during deposition is obtained by correlating the interference fringe pattern of subsequent minima and maxima (m) and the corresponding deposition time. An exponential fit to this data provides the best representation of the deposition rate as depicted in Fig. 2.2. This exponential behavior is expected as the pressure in the gas reservoir decreases with deposition time. The system is cycled through up to about 2.75 interference fringes, corresponding to an ice thickness of 837^{+34}_{-29} nm. The accuracy of the thickness determination is limited by the uncertainty in the literature values of the optical constants, and the incident angle of the laser beam (Baratta & Palumbo 1998). After deposition, the ice thickness is monitored as a function of temperature between 15 to 120 K using different heating rates from 1 to 4 K min^{-1}.

Infrared spectra are obtained with a Fourier Transform Infrared spectrometer (Varian 670-IR FTIR) and recorded in transmission mode between 4000 and 400 cm^{-1} at a resolution of 1 cm^{-1}, co-averaging 256 scans. The samples used for the IR measurements, are grown on the CsI window. The spectrometer is flushed with dry air to minimize background fluctuations due to atmospheric absorptions. Background spectra are acquired at 15 K prior to deposition for each experiment.

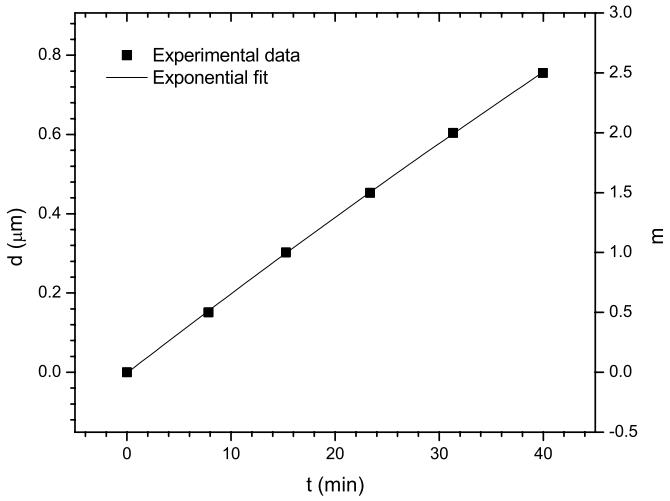

Figure 2.2 – Exponential fit to subsequent interference fringes minima and maxima (m) and the corresponding thicknesses vs. deposition time.

2.3 Results

2.3.1 Interference data and infrared spectra during deposition

Fig. 2.3 shows experimental interference data corresponding to the intensity of the reflected laser beam as a function of ice thickness, collected during a porous ASW growth on the Si substrate. The interference pattern exhibits a small decrease in amplitude with ongoing deposition. This amplitude change can have different reasons; a loss of coherence of the reflected light because of surface roughness, cracks, and/or wide boundaries (Baragiola 2003, Howett et al. 2007, Romanescu et al. 2010). The distance between subsequent minima and maxima is constant within 1% indicating that the density of the porous ASW does not change significantly during deposition (Westley et al. 1998).

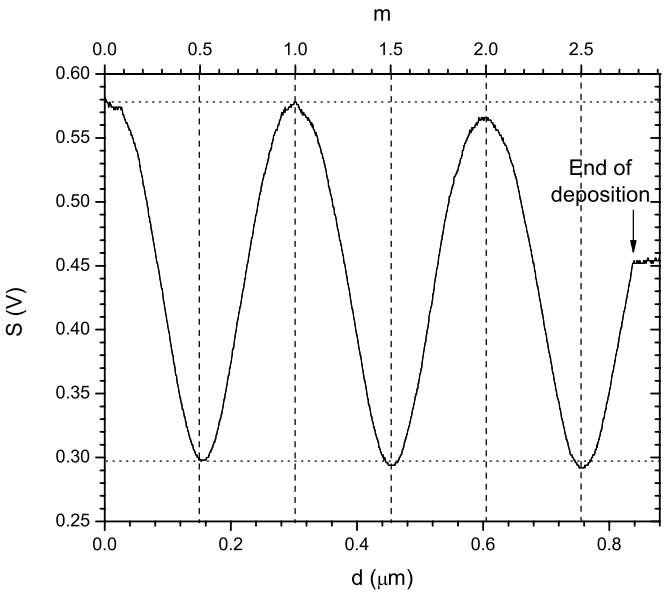

Figure 2.3 – Interference data for porous ASW grown on a Si substrate at 15 K following background deposition. The reflected intensity oscillates between constructive and destructive interference as the ice grows. The deposition is stopped at a point with maximum sensitivity to changes in ice thickness. The error in the thickness measured is about 4%.

The deposition is stopped at the rising slope of the interference pattern (m = 2.75). Change in He-Ne signal can thus be interpreted as change in ice thickness, such that an increasing photodiode signal corresponds to thickening of the ice whereas a decreasing signal corresponds to thinning of the ice.

The FTIR transmission spectra of porous ASW, semi-porous ASW, and crystalline solid water grown on the CsI window are depicted in Fig. 2.4 in the 3760 – 3660 cm^{-1} range that covers the O-H dangling mode of water ice. This mode is used to visualize the

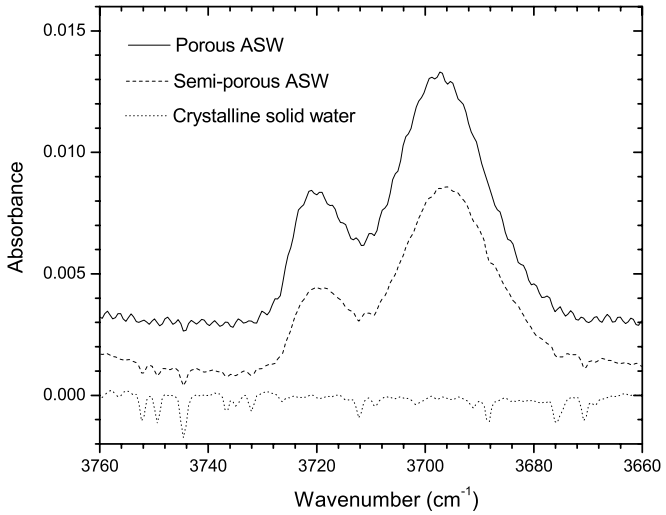

Figure 2.4 – Infrared transmission spectra of the O-H dangling mode of porous ASW, less-porous ASW, and crystalline solid water at 15 K. The absorption band related to the bulk O-H stretching modes has been subtracted and the resulting spectra have been offset for clarity.

level of porosity. To characterize the porosity of each water ice sample, all spectra are corrected with a baseline, and normalized to the bulk O-H stretching modes, located at lower wavenumbers (not shown here). For porous and semi-porous ASW, two absorption bands are found at 3720 and 3696 cm^{-1} that correspond to the O-H dangling mode of the two- and three-coordinate surface-water molecule, respectively. These two bands have been taken as a typical porosity signature (Rowland & Devlin 1991, Rowland et al. 1991), and their intensities reflect the abundance of pores. For crystalline solid water, there is no O-H dangling mode. Therefore, we conclude that at fixed temperature (15 K), the porosity decreases from porous ASW to semi-porous ASW, and from semi-porous ASW to crystalline solid water. Theses results are in good agreement with earlier reports (Stevenson et al. 1999, Kimmel et al. 2001b, Dohnálek et al. 2003, Palumbo 2006), and depict the different morphologies of the deposited samples.

2.3.2 Thermal processing of different ice morphologies

Using optical interference, we can now monitor the thermal evolution of porous ASW, semi-porous ASW, and non-porous crystalline solid water. The results are shown in Fig. 2.5. The corresponding interference data are scaled in order to get the same amplitude between the second constructive interference (m = 2.0) and the third destructive interference (m = 2.5) in the fringe patterns. The small offset is introduced for better visibility. At temperatures above 120 K, diffusion of water molecules becomes significant, and molecules rearrange to a thermodynamically favored crystalline structure (Raut et al. 2008). Hence,

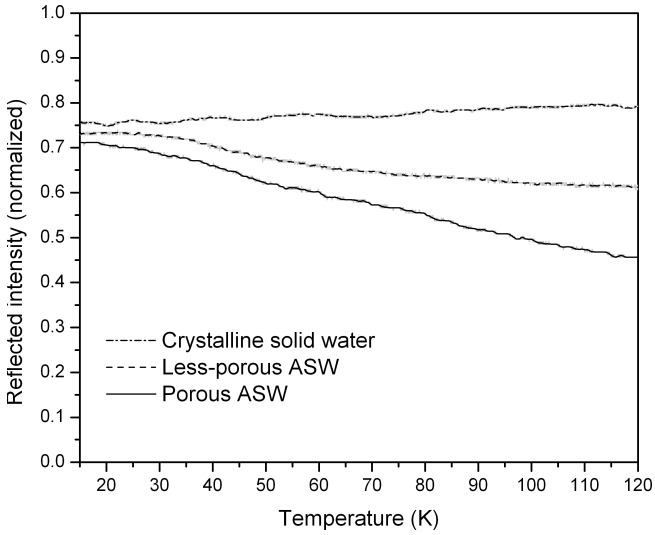

Figure 2.5 – Interference data from the *end of deposition* point onwards (Fig. 2.3), during the thermal annealing experiment on porous ASW, less-porous ASW, and crystalline solid water grown on a Si substrate, with an heating rate set to 2 K min^{-1}. The gray lines represent the raw experimental data, and the black lines are the smoothed data.

we exclude all data at temperatures higher than this threshold.

For crystalline solid water, the He-Ne signal is stable between 15 and 120 K, indicating that the ice thickness remains constant in this temperature range. The result is consistent with the lack of porosity of the sample deposited at 140 K, and then cooled down to 15 K, as confirmed by infrared spectroscopy in Fig. 2.4. For porous ASW, and semi-porous ASW the He-Ne signal does not change between 15 and 20 K. Above 20 K, we observe a gradual drop in the interference signal, which reflects a structural change of the ices; the ices get thinner. Fig. 2.5 shows that the decrease in the signal is stronger for the porous ASW, indicating that the magnitude of the thickness decrease is related to the initial porosity of the sample.

In order to check the temperature dependence of the observed thickness decrease, we monitor the He-Ne beam reflected from porous ASW samples that are warmed up with different heating rates (1, 2, and 4 K min^{-1}). Before each measurement, we use the same background deposition protocol in order to allow accurate comparisons. Fig. 2.6 shows the interference signal for different heating rates. The signal decay as function of temperature is comparable for the different thermal annealing experiments, indicating that the thickness decrease of porous ASW is a fully thermally determined process. Fig. 2.7 shows that the intensity of the O-H dangling feature decreases during the warm-up. This is consistent with the expected porosity loss as discussed in the literature (Baragiola 2003) and references therein; this porosity loss takes place together with the observed thickness decrease.

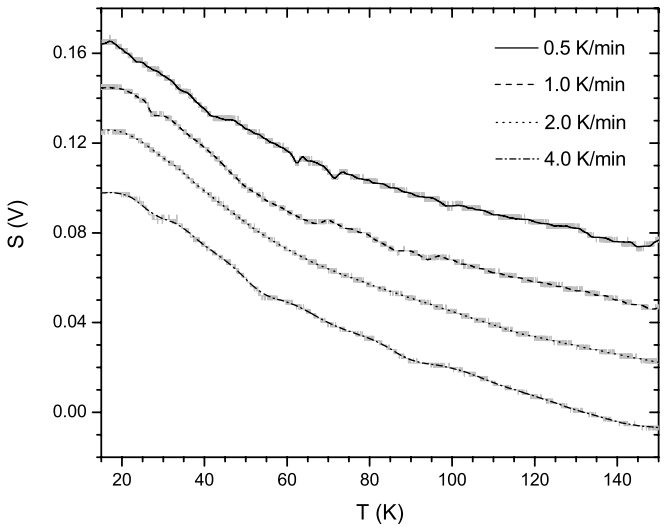

Figure 2.6 – Interference data during the thermal annealing experiment on porous ASW grown on a Si substrate, with different heating rates (1, 2, and 4 K min^{-1}). The gray lines represent the raw experimental data, and the black lines are the smoothed data. The data are offset for clarity. The artifacts in particularly the 0.5 K/min trace are due to laser intensity fluctuations.

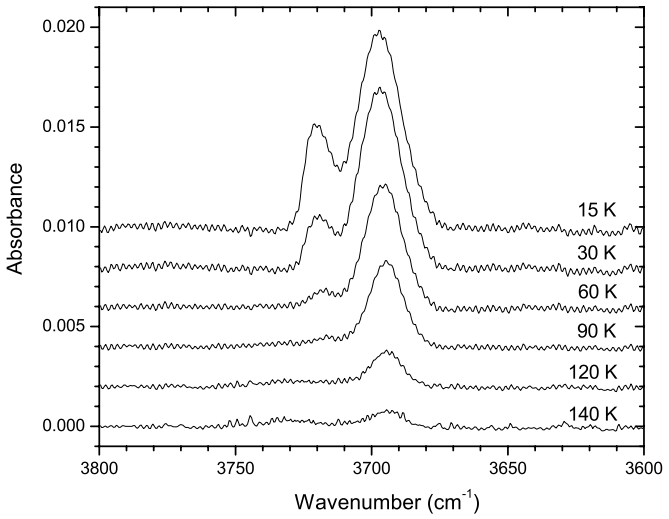

Figure 2.7 – Evolution of the OH dangling modes during annealing of porous ASW from 15 to 120 K. Bulk OH stretching mode has been subtracted and the resulting spectra have been offset for clarity.

2.4 Discussion

Previous work has shown a decrease in both porosity and gas-adsorption capacity of ASW with increasing temperature. We have directly demonstrated here that vapor deposited ASW undergoes a temperature-induced structural change upon heating. A quantitative analysis of the observed thickness decrease in porous ASW is possible by determining the ice thickness at different temperatures. This can be achieved by relating the reflected He-Ne laser intensity $|R|^2$ to the ice thickness during thermal annealing. For layered structures, the reflection coefficient R can be written as a function of the Fresnel reflection coefficients according to the relation (Westley et al. 1998, Dohnálek et al. 2003):

$$R = \frac{r_{01} + r_{12}\, e^{-i2\beta}}{1 + r_{01}\, r_{12}\, e^{-i2\beta}}. \tag{2.2}$$

The Fresnel reflection coefficients r_{01} and r_{12} are associated to the vacuum/ice and ice/substrate interfaces, respectively, and are functions of the refractive indices of vacuum (n_0), ice (n_1), and substrate (n_2). The values of the Fresnel reflection coefficients are given by the following equations and depend on the light polarization. For s-polarized light:

$$r_{01s} = \frac{n_0 \cos\theta_0 - n_1 \cos\theta_1}{n_0 \cos\theta_0 + n_1 \cos\theta_1}. \tag{2.3}$$

$$r_{12s} = \frac{n_1 \cos\theta_1 - n_2 \cos\theta_2}{n_1 \cos\theta_1 + n_2 \cos\theta_2}. \tag{2.4}$$

Snell's law relates the angles of incidence (θ_0, θ_1, and θ_2) with the complex indices of refraction (n_0, n_1, and n_2). We use constant refractive indices $n_0 = 1$ for vacuum, and $n_2 = 3.85 - 0.07i$ for the Si substrate (Mottier & Valette 1981). The refractive index of porous ASW, however, is temperature dependent, and increases linearly from 22 to 120 K; n_1(T) values are available from Dohnálek et al. (2003). We assume that the n_1(T) values obtained depositing the sample at a given temperature are the same as those of the sample warmed up from 15 K to that temperature. The imaginary component, k, is very close to zero (light is not absorbed in the ice film), and can be neglected (Warren 1984, Dohnálek et al. 2003). The exponential term β in Eq. 2.2 describes the phase change of the light as it passes through the ice with:

$$\beta = \frac{2\pi d}{\lambda}\, n_1(\mathrm{T}) \cos\theta_1. \tag{2.5}$$

We assume that the amplitude of the reflected light at a given thickness and temperature is proportional to the photodiode signal (S), with a proportionality constant (A), calculated at 15 K with the initial ice thickness d_0 (here $d_0 = 837$ nm):

$$|R(d_0,\mathrm{T})|^2 = A^{d_0}_{15\,\mathrm{K}} \times S. \tag{2.6}$$

In order to measure the thickness of the ice for other temperatures, we need to take into account the variation of n_1(T) with temperature, and to find the closest root (d) to the

initial ice thickness that satisfies the following equation:

$$|R(d,\mathrm{T})|^2 - \left(A_{15\,\mathrm{K}}^{d_0} \times S\right) = 0. \tag{2.7}$$

Fig. 2.8 shows the calculated ice thickness versus temperature. We find a thickness change for porous ASW from ~833 nm at 20 K to ~733 nm at 120 K, which corresponds to a decrease of 12 ± 1 %. The top and bottom edges of the gray shaded area delimit the error in the initial ice thickness measurement. We observe the same thickness decrease value of about 12% for both upper and lower d_0 values, indicating that the accuracy of the derived thickness change is not strongly affected by the uncertainty of the initial thickness. This derived thickness change is a lower limit since the background accretion of the residual components remaining in the chamber is not explicitly taken into account. The results presented here are confirmed by recent theoretical work; molecular dynamics simulations performed on porous ASW show a thickness decrease of ~10% from 0 to 150 K (Elkind & Fraser 2012). For semi-porous ASW the exact thickness decrease cannot be determined as the n_1(T) values are unknown. Fig. 2.5 indicates that the thickness change is less than for porous ASW, but definitely not zero as for crystalline solid water. The structural collapse of porous ASW is not large in terms of thickness but a decrease of the order of 12% may correspond to a substantial loss in terms of surface area; Bar-Nun & Owen (1998) report an effective surface area loss as large as 90%. The physical mechanism involved during the collapse is poorly understood. It has been proposed that at 38 K, on average, the breaking of one hydrogen bond per molecule becomes possible, restructuring the ice (Jenniskens & Blake 1994, Jenniskens et al. 1995). This is in line with the results found here, with the exception that an onset of a structural change is already observed at 20 K. Our results agree with those of Hagen (1981), who observed irreversible spectral changes in the bulk OH stretching band immediately upon annealing from the 10 K deposition temperature.

The O-H dangling mode characteristic for porous ASW has not been observed in the infrared spectra of interstellar ices, reason why ASW in space is considered to be compact. Previous laboratory experiments are in line with this conclusion, and suggest that over the lifetime of a molecular cloud, pores in interstellar ices are lost upon cosmic ray bombardments (Palumbo 2006, Raut et al. 2008). The present study indicates that a structural change is also realized through heating, i.e., in a protoplanetary disk through radiation from the protostar. This also applies to less-porous ASW.

Upon heating the number of reaction sites becomes scarce, and a chemistry dominated by bulk processes may shift to a chemistry governed by surface processes. A decrease of reaction sites will naturally reduce the reaction efficiency. On the other hand, a low temperature structural collapse may facilitate reactions between adsorbates, and reaction efficiencies will increase with increasing temperature, as the mobility of reacting species gets larger. Gálvez et al. (2010) demonstrated that the thermal processing of porous ASW leads to a marked enhancement of low temperature acid-base reaction yields, in contrast to compact ASW. So far, a thermally induced ice collapse has not been taken explicitly into account in astrochemical models. The situation for mixed ices is likely even more complicated. How do CO or CO_2 affect the water ice structure, morphology, and porosity

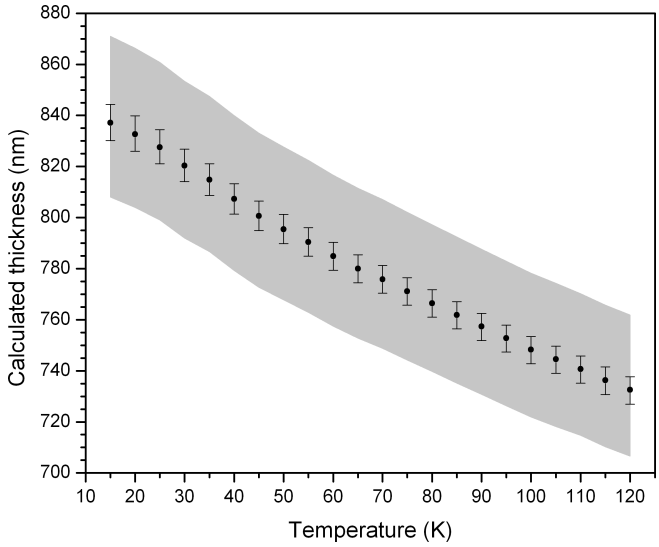

Figure 2.8 – Calculated thicknesses versus temperature during the thermal annealing experiment ($2\,\mathrm{K\,min^{-1}}$) of porous ASW grown on a Si substrate. The vertical bars give the dispersion due to the resolution of the optical interference technique. The gray shaded area takes into account the dispersion due to the error in the initial thickness measured at 15 K.

loss upon heating? With the new technique discussed here, this question can be addressed, as soon as temperature dependent refraction indices have become available.

2.5 Conclusions

We have measured the thickness decrease of porous ASW upon heating for astronomically relevant temperatures, using a new experimental technique, based on optical interference and FTIR transmission spectroscopy.

1. We find for porous ASW a thickness decrease of 12 ± 1 % upon heating from 20 to 120 K. For less-porous ASW this value is lower, and negligible for crystalline solid water.

2. The thickness decrease observed by optical interference is accompanied by the compaction (porosity loss) observed by FTIR.

3. Thermal compaction provides an additional explanation why porous ASW has not been observed in space so far.

4. The observed structural collapse likely will influence the efficiency of the overall chemical solid state network in inter- and circumstellar ices.